Electronic Supplementary Material (ESI) for ChemComm.

Imaging the Electronic Structure of On-Surface Generated Hexacene *(Supporting Information)*

Justus Krüger,[1] Frank Eisenhut,[1] José M. Alonso,[2] Thomas Lehmann,[1] Enrique Guitián,[2] Dolores Pérez,[2] Dmitry Skidin,[1] Florian Gamaleja,[1] Dmitry A. Ryndyk,[1] Christian Joachim,[3] Diego Peña,*[,2] Francesca Moresco,*[,1] Gianaurelio Cuniberti[1]

[1]Institute for Materials Science, Max Bergmann Center of Biomaterials, and Center for Advancing Electronics Dresden, TU Dresden, 01069 Dresden (Germany)

[2]Centro de Investigación en Química Biolóxica e Materiais Moleculares (CIQUS) and Departamento de Química Orgánica, Universidade de Santiago de Compostela, 15782-Santiago de Compostela (Spain)

[3]GNS & MANA Satellite, CEMES, CNRS, 29 rue J. Marvig, 31055 Toulouse Cedex (France)

1. Synthetic details

General methods: All reactions were carried out under argon atmosphere using oven-dried glassware. Solvents were dried by distillation from a drying agent. Commercial reagents were purchased from ABCR GmbH, Aldrich Chemical Co., or Stream Chemicals Inc, and were used without any further purification. *n*-BuLi was used from solution in hexanes (2.40 M). Flash chromatography was performed on Merck silica gel 60 F254. ^{1}H NMR spectra were recorded at 300 or 500 MHz (Varian Mercury instrument). ^{13}C NMR spectra were recorded at 75 or 125 MHz. Low resolution electron impact mass spectra (EI-LRMS) were determined at 70 eV on a HP-5988A instrument. High resolution mass spectra (HRMS) were obtained on a Micromass Autoespec spectrometer.

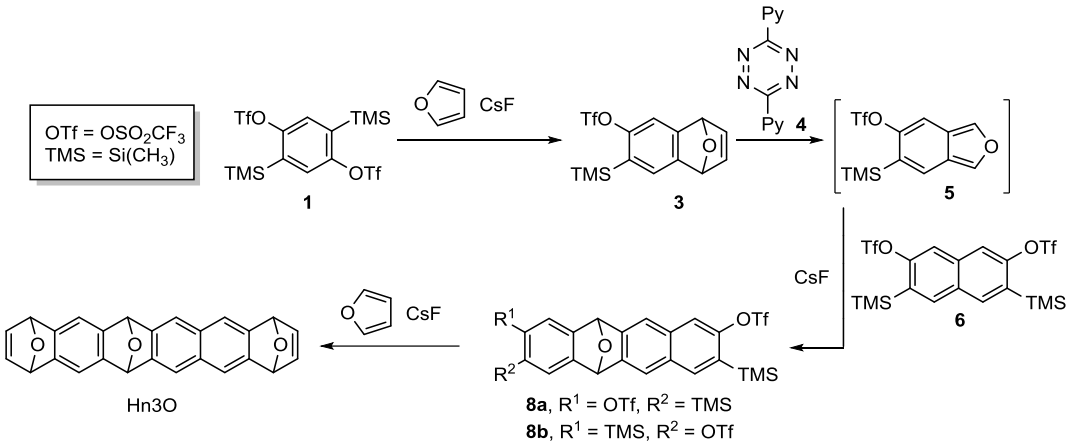

Scheme S1. Synthetic route to obtain hexacene precursors Hn3O.

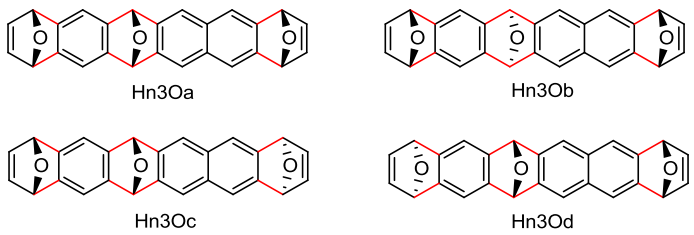

Figure S1. Structures of the four possible triepoxyhexacene (Hn3O) diastereomers. In red the bonds formed by means of Diels-Alder cycloaddition. NMR spectra suggest the formation of a mixture of the four isomers (approximately 1:1:1:1 ratio, see Figures S11 and S12). Attempts to separate these diastereomers by column chromatography were unsuccessful.

1.1. Synthesis of triflate 3

CsF (132 mg, 0.87 mmol) was added over a solution of bistriflate **1**[1] (300 mg, 0.58 mmol) and furan (84 µL, 1.16 mmol) in dry MeCN (5.7 mL). The mixture was stirred 60 min at 45ºC. After evaporation of the solvent under reduced pressure, the residue was purified by column chromatography (hexane/AcOEt 7:3) yielding **3** as a colorless solid (150 mg, 76%)

^{1}H NMR ($CDCl_3$, 300 MHz), δ: 0.34 (9H, s), 5.72 (2H, s), 7.07-7.02 (2H, m), 7.24 (1H, s), 7.33 (1H, s) ppm. ^{13}C NMR ($CDCl_3$, 75 MHz), δ: -0.8 (CH_3), 81.9 (CH), 82.2 (CH), 113.0 (CH), 118.8 (q, *J* = 321 Hz, CF_3), 126.1 (CH), 128.4 (C), 142.6 (CH), 143.2 (CH), 148.1 (C), 152.3 (C), 153.7 (C) ppm. EM (EI+), m/z (%): 364 (M, 17), 149 (5), 177 (100). HRMS: for $C_{14}H_{15}O_4F_3SiS$ calculated 364.0412, observed 364.0413. Mp: 69.9-70.8ºC.

1.2. Synthesis of bistriflates 8a and 8b

A solution on triflate **3** (91 mg, 0.251 mmol) and 3,6-di-2-pyridyl-1,2,4,5-tetrazine (**4**, 59 mg, 0.251 mmol) in dry MeCN (2.1 mL) was stirred at 45 ºC for 90 min. After that time, a solution of bistriflate **6**[2] (100 mg, 0.176 mmol) in MeCN (1 mL) and CsF (40 mg, 0.264 mmol) were sequentially added, and the mixture was stirred at 45 ºC for 16 h. After evaporation of the solvent under reduced pressure, the residue was purified by column chromatography (hexane/AcOEt 8:1) yielding the mixture **8a**-**b** as a colorless oil. NMR showed a mixture of non-separable isomers (50 mg, 42%).

Spectroscopic data of the mixture:

^{1}H NMR ($CDCl_3$, 300 MHz), δ: 0.31-0.39 (36H, m), 6.21 (4H, s), 7.38 (2H, m), 7.48 (2H, m), 7.70 (2H, br s), 7.72 (2H, m), 7.76-7.80 (2H, m), 7.89-8.01 (2H, m) ppm. ^{13}C NMR ($CDCl_3$, 75 MHz), δ: -0.9, -0.8, 81.7, 81.9, 112.7, 112.9, 117.2, 117.3, 118.8 (q, *J* = 321 Hz), 118.9, 119.1, 119.3, 119.5, 121.1, 125.8, 127.0, 127.2, 130.8, 131.4, 131.5, 133.4, 133.5, 137.2, 137.3, 144.2, 144.5, 144.8, 145.1, 145.9, 146.1, 151.0, 151.2, 153.1 ppm. EM (EI+), m/z (%): 684 (M, 100), 669 (M-15, 20). HRMS: for $C_{26}H_{26}O_7F_6Si_2S_2$ calculated 684.0563, observed 684.0565.

1.3. Synthesis of hexacene precursors Hn3O

CsF (106 mg, 0.70 mmol) was added over a solution of the mixture **8a**-**b** (60 mg, 0.09 mmol) and furan (260 µL, 3.52 mmol) in MeCN (2.3 mL). The mixture was stirred at 45ºC for 16h. After cooling down the mixture, the solvent was evaporated and the residue was purified by column chromatography (hexane/AcOEt 1:1) yielding Hn3O as a white solid (20 mg, 40%). ^{1}H NMR showed a 1:1:1:1 mixture of four non separable diastereoisomers.

^{1}H NMR ($CDCl_3$, 500 MHz), δ: 5.57-5.62 (8H, m), 5.74-5.76 (8H, m), 6.04-6.06 (8H, m), 6.87-6.92 (8H, m), 6.96-7.03 (8H, m), 7.23-7.27 (8H, m), 7.47-7.49 (8H, m), 7.53-7.54 (8H, m) ppm ^{13}C NMR ($CDCl_3$, 125 MHz), δ: 81.8, 81.9, 81.9, 81.9, 82.2, 82.2, 82.3, 82.3, 82.3, 82.3, 82.4, 113.5, 113.6, 113.8, 113.9, 119.0, 119.0, 119.1, 119.1, 119.2, 130.4, 130.4, 130.5, 141.9, 141.9, 142.0, 142.0, 143.2, 143.3, 143.3, 143.4, 144.7, 144.8, 145.0, 145.1, 145.2, 145.2, 145.3, 145.8, 145.8, 145.9, 146.0, 148.7, 148.8, 148.9, 149.0 ppm. EM (ESI-FIA-TOF), m/z (%): 377 (M+1, 100). HRMS: for $C_{26}H_{16}O_3$ calculated 376.1197, observed 376.1167.

2. STM imaging

STM experiments were performed using a custom-built instrument operating at a low temperature of T = 5 K and ultra-high vacuum (p ≈ 1 × 10^{-10} mbar) conditions. STM measurements were usually performed in constant-current mode with the bias voltage applied to the sample. Differential conductance spectra were measured using lock-in detection with a modulation frequency of 833 Hz and a modulation amplitude of 20 mV. Only those tips showing the Au(111) surface state[3] at -0.51 V were used for spectroscopy measurements on the molecules. For STS measurements of single molecules, the tip was stabilized at a desired position with the surface-tip distance determined by applied bias and set tunneling current. Subsequently, the feedback loop was turned off and the voltage was swept in the desired bias range while simultaneously recording tunneling current and the differential conductance signal as function of the bias.
An Au(111) single crystal was used as substrate and prepared by repeated cycles of sputtering (Ne+) and annealing (720 K). After cleaning, the molecular precursors of hexacene were deposited (sublimation temperature of 160 °C) from a quartz crucible in a Knudsen cell onto the surface kept at room temperature. The sample was then annealed at 120 °C for 5 min, transferred into the STM and cooled down to cryogenic temperature. Subsequent temperature-induced experiments were carried out by transferring the sample out of the STM to anneal at the respective temperature for 5 min. Subsequently, the sample was cooled again and transferred back inside the microscope without breaking the ultra-high vacuum at any time. CO molecules were deposited with a very low surface coverage onto the cold sample (T ≈ 10 K) and then deliberately picked up by the tip of the STM to functionalize the apex.[4]

3. Computational details

Ab initio density functional theory (DFT) calculations were performed using a mixed Gaussian and plane wave approach implemented in the Quickstep code of CP2K.[5] Goedecker-Teter-Hutter pseudo potentials[6] with the Perdew-Burke-Ernzerhof exchange-correlation functional[7] and a valence double-zeta basis set were chosen. Dispersion correction was included by using the nonlocal revised Vydrov-van Voorhies (rVV10) functional.[8] It goes beyond pairwise correction schemes by adding a nonlocal correlation term to the exchange functional and describes accurately the adsorption geometries for acenes. DFT was used to study the adsorption of hexacene and the relevant intermediates and precursors. The Au(111) surface was modelled by a periodic slab of six layers, with the three bottom layers fixed at bulk positions during relaxation. Surface reconstruction effects were neglected. By exploring the potential energy surface at several adsorption sites, the minimum energy adsorption configuration was found for the molecule.

For the computation of dI/dV maps we applied the mono-electronic elastic scattering quantum chemistry (ESQC) approach.[9] This technique employs a single-electron Hamiltonian to describe the electronic structure of the STM tunneling junction within the extended Hückel theory and the scattering matrix approach. It allows to obtain constant-height and constant-current STM images and differential conductance maps including local tip apex interaction with the electronic cloud of the molecule. For comparison with experimental dI/dV maps, constant-current maps of the differential conductance at resonance energies of the respective molecular states were calculated.

4. Additional STM data

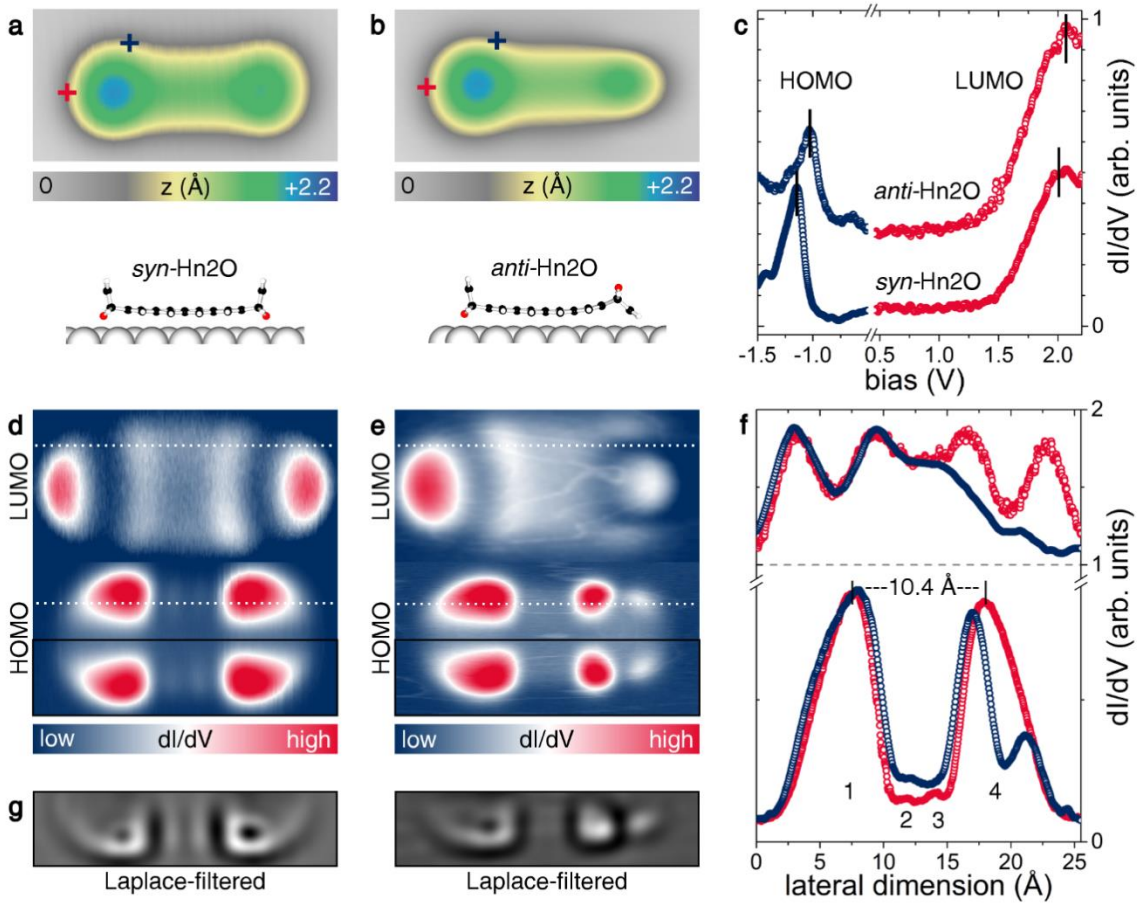

Figure S2. Structure and electronic properties of intermediates Hn2O on Au(111). (a and b) STM images (V = +0.5 V, I = 30 pA) of *syn*- and *anti*-Hn2O, respectively. Additionally, the adsorption configuration of both is shown as derived by DFT. (c) dI/dV spectra of *syn*- (lower curve) and *anti*-Hn2O (upper) taken on the position as indicated by blue and red marks. Spectra are shifted vertically for clarity. (d) dI/dV maps for *syn*-Hn2O at +2.0 V (top), -1.15 V (down), and I = 0.1 nA. (e) dI/dV maps for *anti*-Hn2O +2.05 V (top), at -1.05 V (down), and I = 0.2 nA. All image sizes are 13 Å x 26 Å. (f) Extracted line scans along the dI/dV maps as indicated by white dashed lines in the images in d and e. The curves were normalized and shifted for clarity. (g) Laplace-filtered images of lower half of HOMO maps.

Our experimental approach allowed us to study also the properties of key intermediates, which rationalize the on-surface generation via the structural and electronic differences compared to hexacene. After cleaving the oxygen at the middle position from the precursors, the resulting molecular intermediates Hn2O (see Figure 1b) feature an aromatic system of four linearly fused benzene rings at the center. This system is electronically confined due to C-C bonds to sp3 hybridized carbon atoms and structurally framed within two upstanding units on either side of the molecule. Depending on the orientation of the two 1,4-epoxy groups with respect to each other, one can further distinguish *syn* and *anti* diastereomers of Hn2O. Both were imaged on Au(111) as dumbbell-shaped

protrusions, which can be seen in the STM images in Figure S2a and S2b. There is, however, a notable difference between the topography of both species, as the *syn* configuration is symmetric in its extent, the *anti* diastereomer shows one tapered part. This side coincides with a single oxygen atom facing away from the surface, while the broad part of the dumbbell is related to the fact that two CH groups are pointing towards the tip on this side of the molecule.

By probing the differential conductance in terms of point spectroscopy at edge positions of the molecular topography, clear resonances could be singled out for both diastereomers as shown in Figure S2c. In the case of *syn*-Hn2O, the corresponding bias values for the HOMO and LUMO level are at -1.15 V and +2.00 V, respectively. These values are shifted to slightly larger values for *anti*-Hn2O and account for -1.05 V and +2.05 V. Nevertheless, the HOMO-LUMO gap is similar for both diastereomers and distinctly larger compared to the energy gap of hexacene. This is in line with a simple model of a larger energy level spacing for a stronger spatial confinement of the frontier orbitals.

The constant-current images of the differential conductance at the respective resonance energies are depicted in Figure S2d and S2e. Notably, the maps for *syn*-Hn2O reveal that the recorded images of the molecular frontier orbitals are symmetric with respect to two axes, despite the fact that the simultaneously acquired topography image (Figure S2a) shows an asymmetry of the apparent height of the two maxima. On the contrary, the dI/dV maps for the LUMO and HOMO of the *anti* diastereomer display two dissimilar sides as one would expect from the asymmetric molecule configuration.

More importantly, features of the planar adsorbed tetracene-like backbone can be recovered within the electronic structure of the *syn*-diastereomer. Figure S2d demonstrates that the spatial distribution of the four strongest conductance peaks of the HOMO appears not extended over the whole molecule but is strongly confined to the central part with a peak-to-peak distance of 10.4 Å along the long axis. Besides these four major lobes, one can also identify four very faint inner lobes (cf. line scans in Figure S2f and Laplace-filtered image in Figure S2g). This results in a molecular orbital pattern which is a clear fingerprint of the four aromatic rings. Bearing in mind the stronger curvature of the aromatic backbone for the adsorbed *anti*-diastereomer, it is not surprising that similar features remain hidden in the respective image of the HOMO.

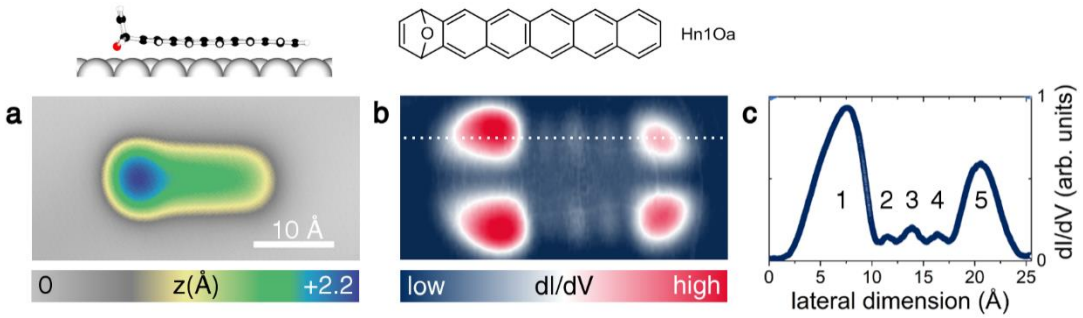

Figure S3. STM imaging of intermediate Hn1Oa on Au(111). (a) Constant-current image acquired at V = +0.1 V and I = 40 pA. (b) Constant-current (I = 0.1 nA) map of the differential conductance at V = -0.85 V, corresponding to the HOMO resonance of Hn1Oa. Image size: 13 Å x 26 Å. (c) Line scan along upper half of HOMO map as indicated by dashed line in b. Ten lobes are in total visible resembling the pentacene-like aromatic backbone.

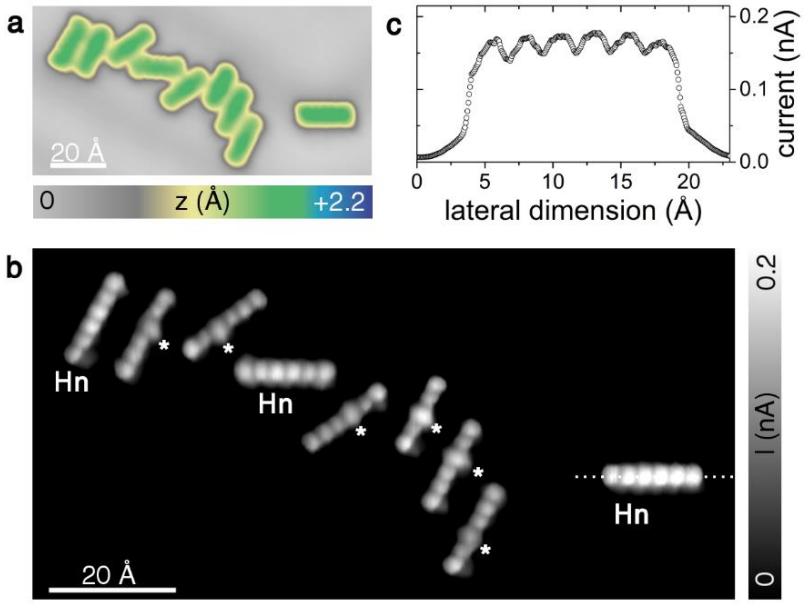

Figure S4. Surface after annealing at 150 °C. (a) Constant-current image (V = -0.7 V, I = 50 pA) acquired with a CO-functionalized tip. (b) Constant-height measurement with a CO-tip and at an applied bias of V = -5 mV. The tip height was stabilized over the bare surface with a set point of V = -0.7 V and I = 10 pA and then decreased by 2.2 Å. Hexacene as well as Hn1Ob are present and can be distinguished by different contrast at the third benzene ring (marked by star). (c) Current trace along main axis of individual hexacene (dashed line in b) reveals sub-molecular corrugation.

Figure S4 presents a typical constant-current STM image after annealing the Au(111) sample at 150 °C indicating that molecules with pronounced dumbbell-shape were not observed anymore. This suggests that the two oxygen atoms at the outer positions were very effectively reduced from the precursors. However, we could also recognize that not all the molecules show the same flat topography after annealing at 150 °C and attribute slight deviations to the fact the oxygen atom at the middle position was not reduced from all precursors. Imaging the surface area with a CO-functionalized tip at constant height (cf. Figure S4b) allowed us to obtain a higher resolution and to disentangle the true nature of the resulting states. Hexacene molecules were imaged with a sub-molecular corrugation which is shown by the line scan of Figure S4c. Closer inspection of the constant-height images led to the conclusion that a fraction of molecules showed a different contrast at their third benzene ring (marked with a star in Figure S4b) which is most likely related to the attached middle oxygen and matches the structure of the intermediate Hn1Ob (see Figure 1b in the main text). Separation of the remaining oxygen might only be obtained with considerably higher annealing temperatures to increase diffusion and reactivity. Thus, the orientation of the remaining oxygen was assumingly pointing away from the surface resulting in a weak oxygen-metal interaction, which limits the hexacene generation.

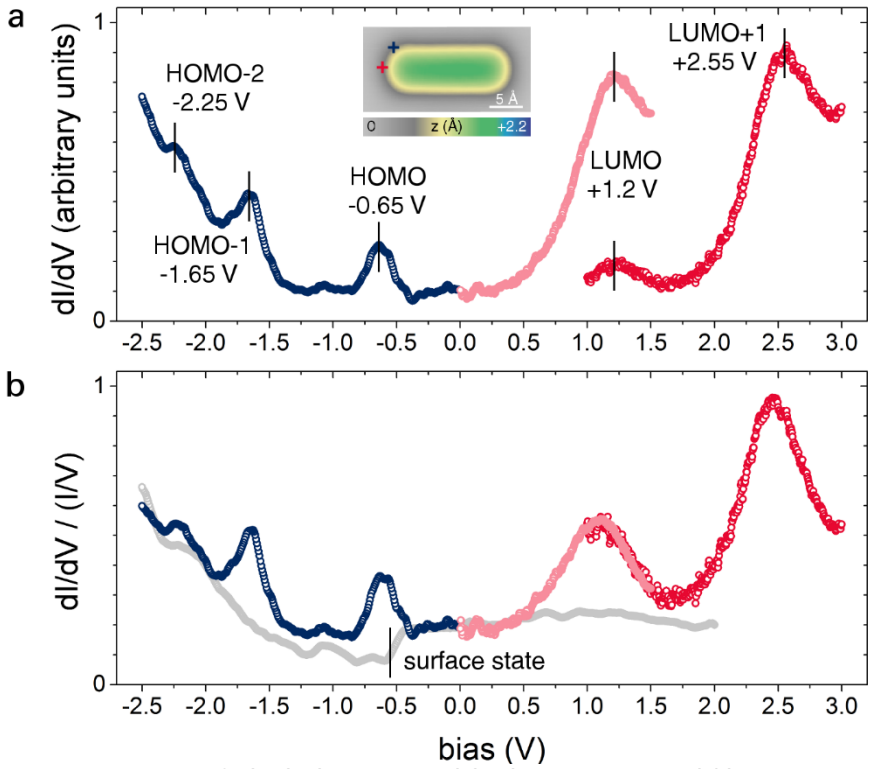

Figure S5. STS measurements of single hexacene. (a) Three separate dI/dV spectra recorded at constant height; the blue spectrum was taken on the corner position while the red curves were acquired at the end position of the molecule as indicated by the STM image (V = +0.2 V, I = 30 pA) in the inset. Tip heights were stabilized at V = +1 V and, from the left, I = 0.15 nA, 0.15 nA and 0.06 nA. (b) Normalized differential conductance (differential conductance multiplied by tunneling resistance) for the three respective molecule spectra as well as for one measurement of the bare surface (grey curve).

5. Additional ESQC data

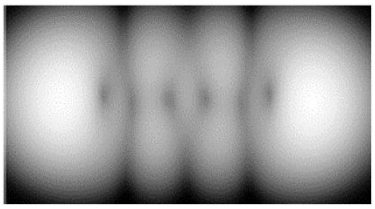

Figure S6. Calculated pure HOMO-2. Calculated differential conductance map of the mono-electronic HOMO-2 resonance using ESQC, demonstrating that a superposition of several tunneling current distributions is necessary to reproduce the experimental observation.

6. NMR data

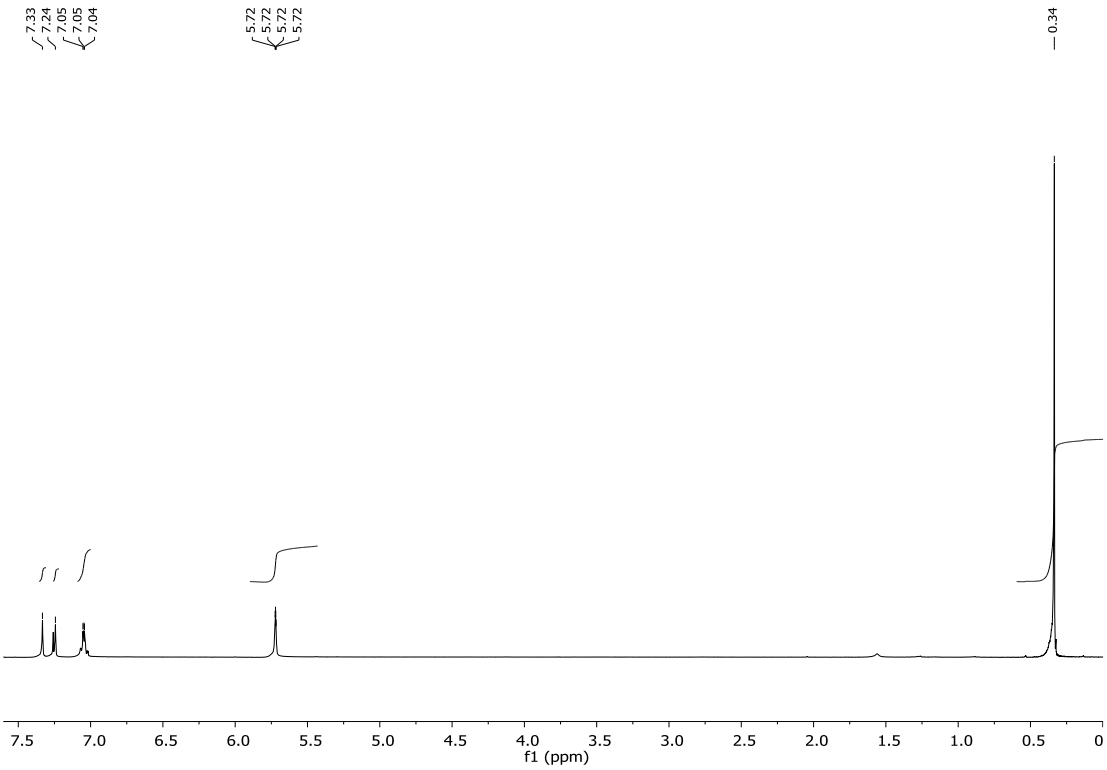

Figure S7. ^{1}H NMR of compound **3**.

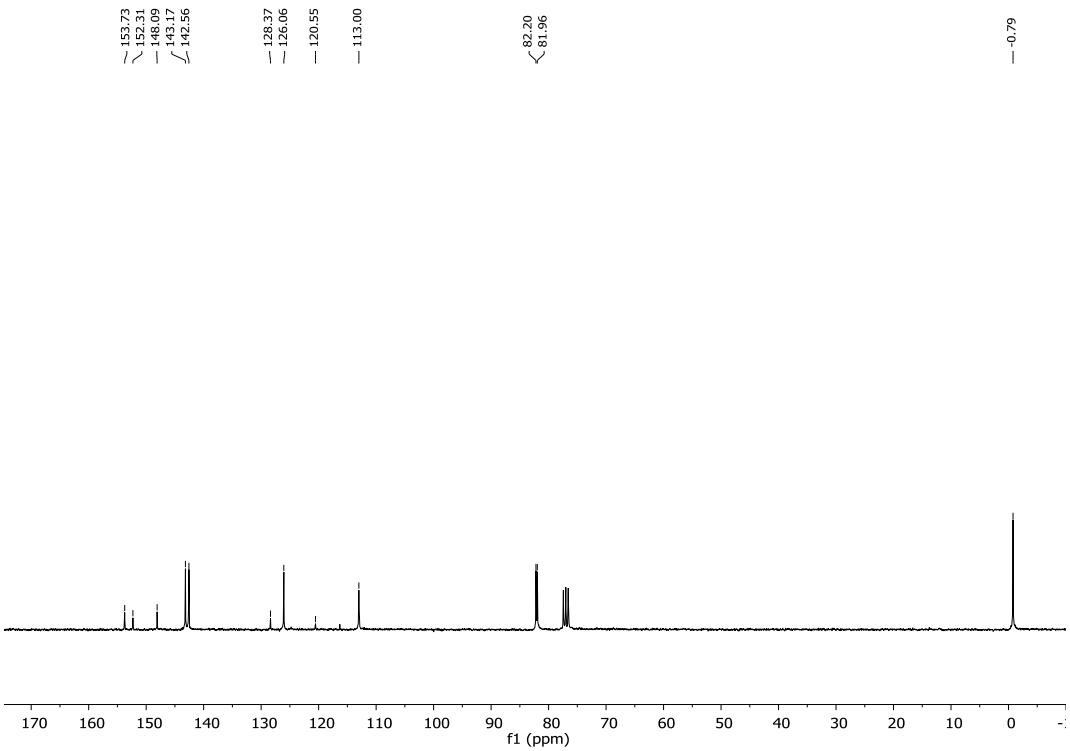

Figure S8. ^{13}C NMR of compound **3**.

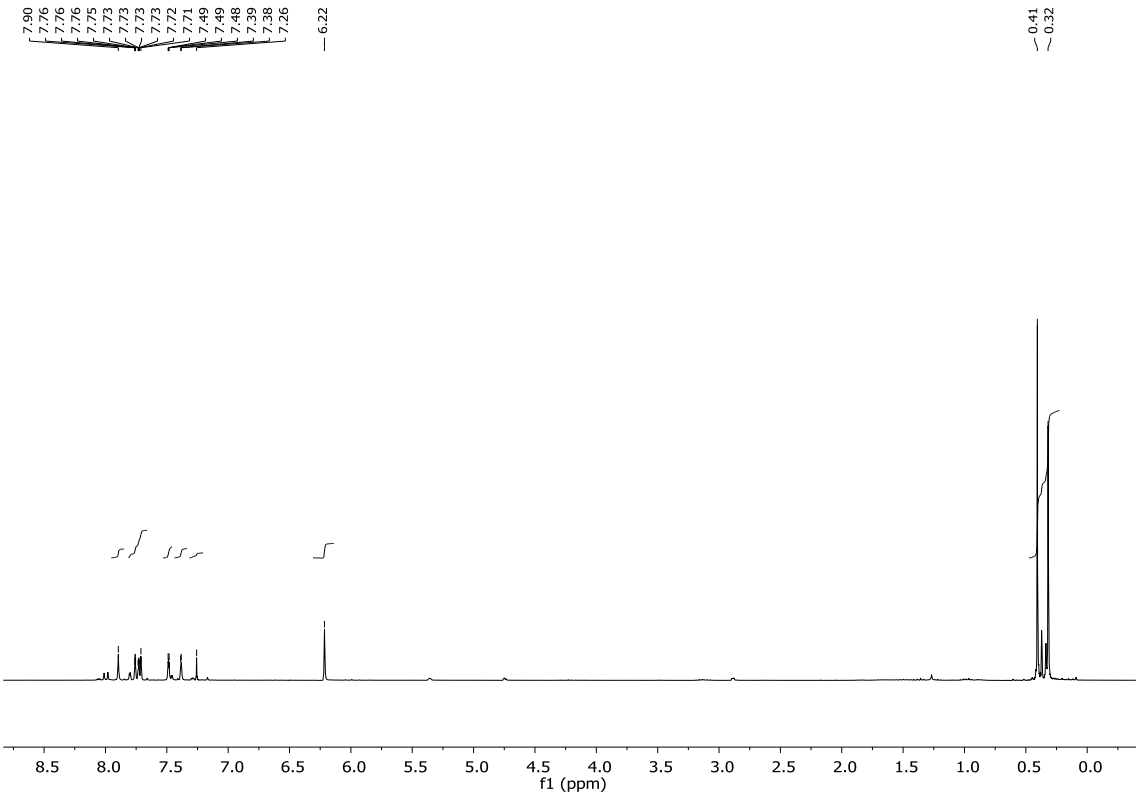

Figure S9. ^{1}H NMR of **8a**-**b**.

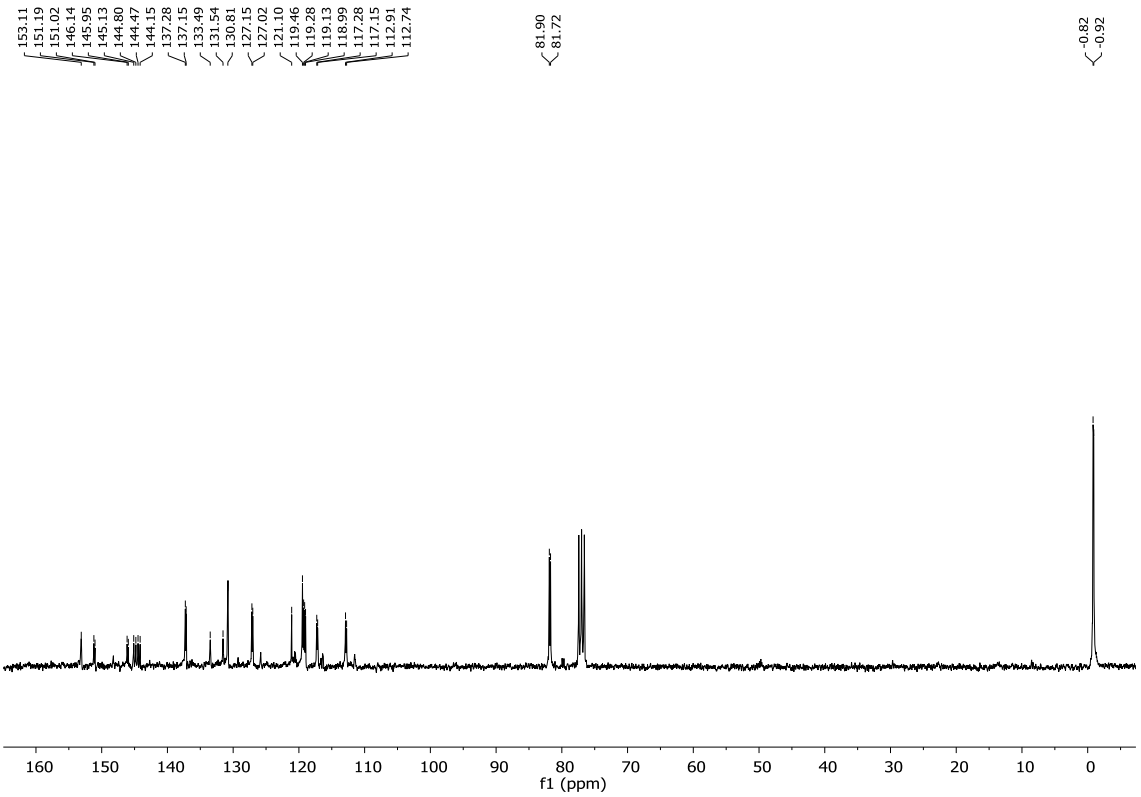

Figure S10. ^{13}C NMR of **8a**-**b**.

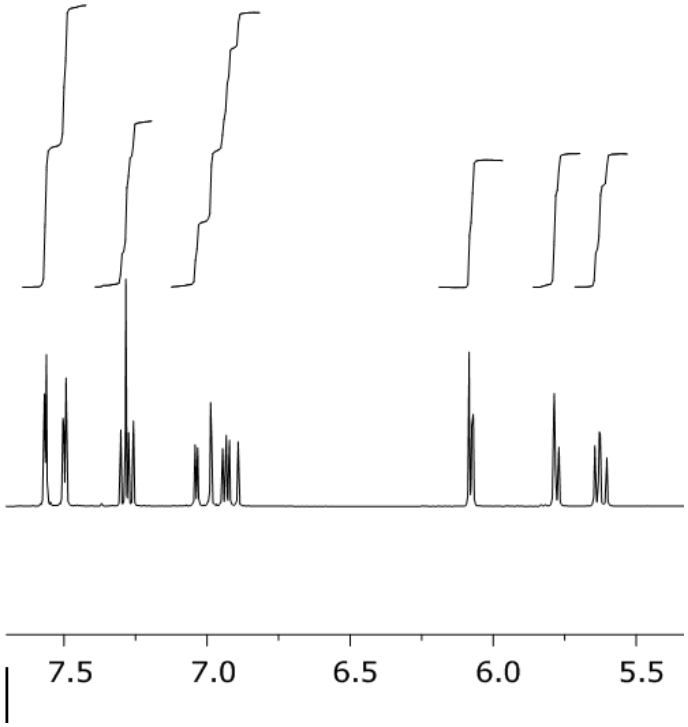

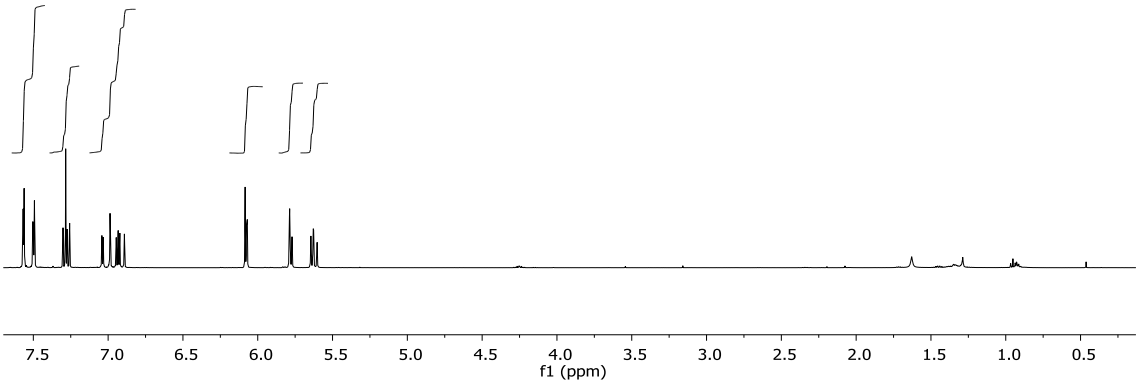

Figure S11. ^{1}H NMR of Hn3O (mixture of four diastereomers).

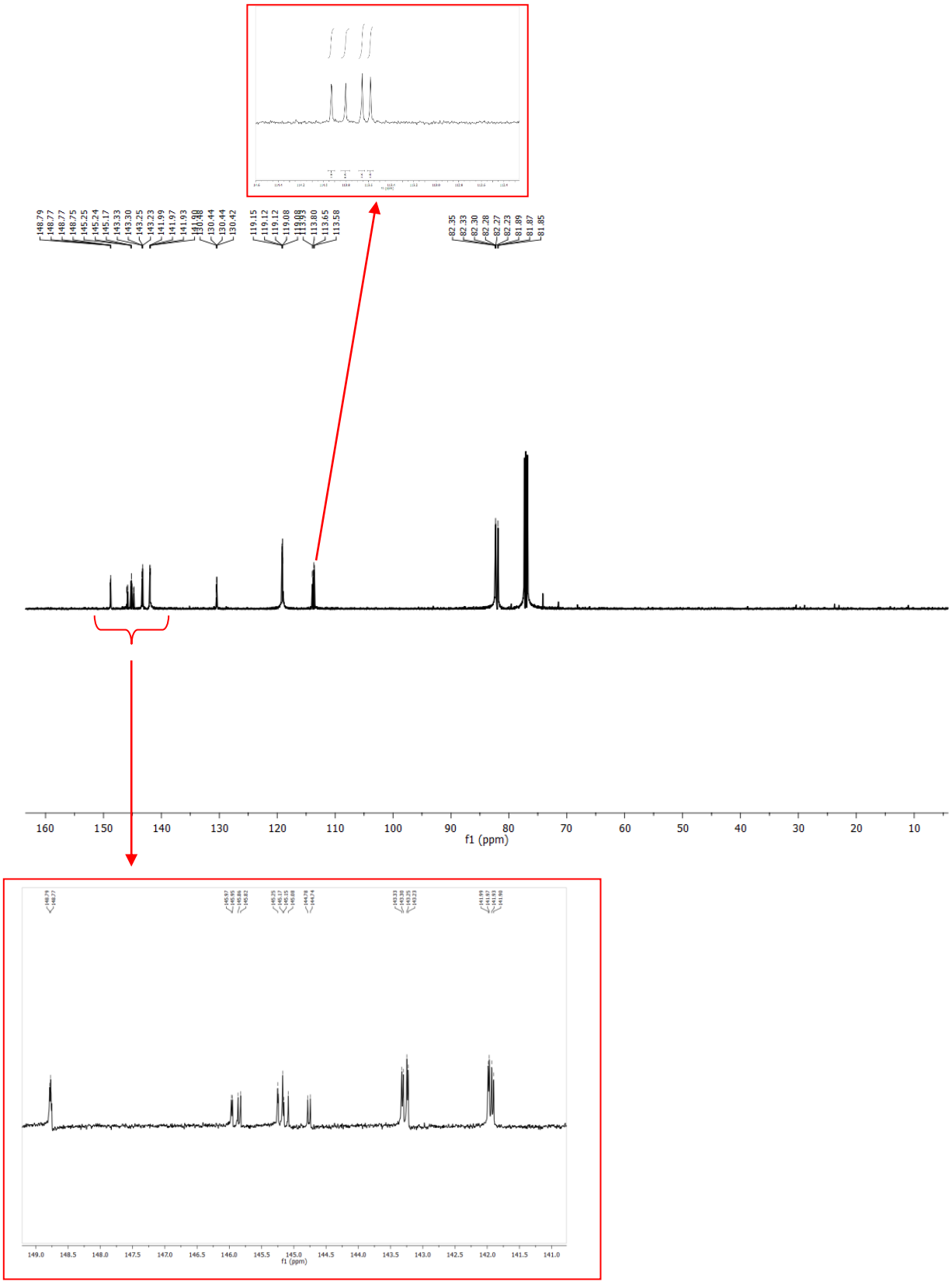

Figure S12. ^{13}C NMR of Hn3O. Most signals split in four peaks due to the presence of four diastereomers (*ca*. 1.1:1:1:1 ratio).

7. References

[1] H. M. Duong, M. Bendikov, D. Steiger, Q. Zhang, G. Sonmez, J. Yamada, F. Wudl, *Org. Lett.* **2003**, *5*, 4433-4436.

[2] C. Kitamura, Y. Abe, T. Ohara, A. Yoneda, T. Kawase, T. Kobayashi, H. Naito, T. Komatsu, *Chem. Eur. J.* **2010**, *16*, 890-898.

[3] W. Chen, V. Madhavan, T. Jamneala, M. F. Crommie, *Phys. Rev. Lett.* **1998**, *80*, 1469-1472.

[4] L. Bartels, G. Meyer, K.-H. Rieder, *Appl. Phys. Lett.* **1997**, *71*, 213-215.

[5] J. VandeVondele, M. Krack, F. Mohamed, M. Parrinello, T. Chassaing, J. Hutter, *Comput. Phys. Commun.* **2005**, *167*, 103-128.

[6] S. Goedecker, M. Teter, J. Hutter, *Phys. Rev. B* **1996**, *54*, 1703-1710.

[7] J. P. Perdew, K. Burke, M. Ernzerhof, *Phys. Rev. Lett.* **1996**, *77*, 3865-3868.

[8] R. Sabatini, T. Gorni, S. de Gironcoli, *Phys. Rev. B* **2013**, *87*, 041108.

[9] P. Sautet, C. Joachim, *Chem. Phys. Lett.* **1988**, *153*, 511-516.